HHS Public Access

Author manuscript

Leukemia. Author manuscript; available in PMC 2023 March 02.

Published in final edited form as:

Leukemia. 2023 January ; 37(1): 235–239. doi:10.1038/s41375-022-01753-4.

Discriminating activities of DEAD-Box Helicase 41 from myeloid malignancy-associated germline variants by genetic rescue

Jeong-Ah Kim[1], **Siqi Shen**[2], **Daniel R. Matson**[1], **Lauren N. Lovrien**[3], **Kelcy J. Smith-Simmer**[4], **Sunduz Keles**[2], **Jane E. Churpek**[3], **Emery H. Bresnick**[1]

[1]Wisconsin Blood Cancer Research Institute, Department of Cell and Regenerative Biology, Carbone Cancer Center, University of Wisconsin School of Medicine and Public Health, Madison, WI, USA;

[2]Department of Biostatistics and Biomedical Informatics, Carbone Cancer Center, University of Wisconsin School of Medicine and Public Health, Madison, WI, USA;

[3]Division of Hematology, Oncology, and Palliative Care, Department of Medicine, University of Wisconsin School of Medicine and Public Health, Madison, WI, USA;

[4]Department of Pediatrics, University of Wisconsin School of Medicine and Public Health, Madison, WI, USA

To the Editor:

Heterozygous DDX41 germline variants generate a predisposition for the development of myelodysplastic syndrome (MDS) and acute myeloid leukemia (AML). Patients present with cytopenias, bone marrow hypocellularity, erythroid dysplasia and/or myeloid malignancy[1]. Although DEAD-box helicase 41 (DDX41) is implicated in oncogenic and innate immune mechanisms, there are many unanswered questions about how the ever-increasing spectrum of genetic variants impact DDX41 activity. Assays to discriminate *DDX41* variants of undetermined significance from pathogenic variants, which is fundamental for clinical genetic curation, have not been reported, thus limiting the clinical utility of genetic information. Here, we describe a facile genetic rescue assay that discriminates activities of DDX41 from those of human myeloid malignancy-associated germline and somatic DDX41 mutants.

DDX41, a highly conserved member of the RNA helicase family of metazoan proteins[2], exerts post-transcriptional and translational functions, including the regulation of pre-mRNA

Correspondence to Emery H. Bresnick, ehbresni@wisc.edu; Jane E. Churpek, jchurpek@wisc.edu.

Author Contributions

J.K. and E.H.B. designed the study and wrote the manuscripts with input from the other authors. J.K. and J.E.C. performed experiments and analyzed data. D.R.M. facilitated antibody generation. S.S. and S.K. conducted statistical and computational analyses of RNA-seq data. J.E.C., L.L. and K.S.S. were responsible for patient identification and consent and clinical data collection and analysis.

Competing Interests

The authors declare no competing interests.

Supplementary Information

Supplementary information consists of Figure 1, Table 1 (PDF) and Table 2 (Excel file).

splicing and ribosomal RNA transcription[3]. DDX41 senses intracellular DNA in the cGAS-STING pathway[4], maintains genomic stability at transcriptional loci harboring R-loops[5] regulates inflammatory gene expression[4] and controls snoRNA processing in mouse leukemic stem/progenitor cells[6].

We identified two rare *DDX41* variants of uncertain significance in two unrelated families (Fig. 1A and Supplementary Table 2). In family 1 (Fig. 1A upper), the proband with p.Lys331del was diagnosed with melanoma at age 43 and low platelets in the context of a normal bone marrow examination at age 66. His mother was diagnosed with low platelets at age 77 and MDS with excess blasts-1 with a normal karyotype and *DDX41* p.Lys331del (VAF 83%) at age 82. Her three brothers and three sisters were diagnosed with low platelets or leukemia after their 60s. In family 2 (Fig. 1A lower), the proband carried germline p.Arg293His. His father was diagnosed with normal karyotype MDS at age 62. He quickly progressed to AML and passed away after allogeneic stem cell transplantation. Both variants occur within the well-conserved DEAD-box domain (Fig. 1B). Sanger sequencing of genomic DNA confirmed *DDX41* sequence variation (Fig. 1C).

To predict whether deletion or substitution of these residues may disrupt DDX41 three-dimensional structure, we utilized AlphaFold[7]. As with the previously reported *DDX41* recurrent germline variant (Gly173Arg[8]) and the common somatic variant (Arg525His[9, 10]), the gross structural features of the variants are predicted to resemble wild type (WT) DDX41 (Fig.1E). The modeling predicts that DDX41 Arg293 forms hydrogen bonds surrounding Leu291, His315, Met316, His312, and Gly313 residues. With the histidine substitution of this residue (R293H), the guanidino group is replaced with an imidazole ring, which is predicted to abrogate hydrogen bonding with Leu291, His312, and Gly313 residues (Fig.1D, upper right). Hydrogen bond disruption was also predicted for the p.Arg525His (R525H) variant. While Arg525 is predicted to form hydrogen bonds with Gly521, Asp497, and Asn528, the Arg525His variant might lose hydrogen bonds with Gly521 and Asp497 (Fig.1D, upper left). Lys331 can form hydrogen bonds with Leu328 and Gln329. The lysine 331 deletion (K331del) is predicted to disrupt hydrogen bonding with Gln329 (Fig.1D, lower right). Since intramolecular hydrogen bonds stabilize protein conformations, in principle, altered intramolecular interactions may alter DDX41 function.

Myeloid malignancy occurring in the context of *DDX41* germline variants feature a late age of onset and often acquire an additional somatic *DDX41* mutation[11]. Given these attributes and lethality in homozygous knockout mice[6] prior studies to dissect DDX41 mechanisms have been conducted with heterozygous knockout mice, in conjunction with aging or the acquisition of a somatic mutation[6]. As ascribing mechanistic consequences of variants in proteins that profoundly influence cellular functions can be complex, we developed an assay to enable facile mechanistic dissection and clinical curation of *DDX41* variants (Fig. 2A) as a complement to complex *in vivo* strategies. The assay utilizes Hoxb8-immortalized mouse fetal liver progenitor cells, which exhibit a normal myeloid progenitor cell phenotype[12]. These cells were engineered with CRISPR-Cas9 to generate $Ddx41^{+/-}$ clonal lines with reduced endogenous DDX41 protein levels. Analogous to our GATA2 rescue systems[12–14], WT or mutant DDX41 proteins can be expressed at near-physiological levels and functional consequences *e.g.,* impact on transcript levels, quantified. The crRNA target sequences

resided upstream of the exon encoding functional domains (exon 3 (A)), or within exons encoding the N-terminal DEAD-box domain (exon 6 (B) and exon 8 (C), Fig. 2B). We validated the *Ddx41*$^{+/-}$ cells by Sanger sequencing of genomic DNA at and surrounding the target sequence (Fig. 2C). Semi-quantitative western blotting revealed reduced DDX41 levels in hi-*Ddx41*$^{+/-}$ relative to hi-*Ddx41*$^{+/+}$ cells (Fig. 2D). hi-*Ddx41*$^{+/+}$ and hi-*Ddx41*$^{+/-}$ cells were infected with retrovirus expressing GFP alone (Empty) or GFP with DDX41 or myeloid malignancy-associated DDX41 variants. After two days, GFP-positive cells were sorted and analyzed by western blotting (Fig. 2E, F). Importantly, the proteins were not overexpressed, as the aggregate level of DDX41 and the DDX41 variant in hi-*Ddx41*$^{+/-}$ cells resembled that of hi-*Ddx41*$^{+/+}$ cells (Fig.2F).

DDX41 has three putative NLS sequences and localizes to the nucleus in the steady-state[15]. All disease-associated variants tested were nuclear-localized, resembling DDX41. Thus, the sequence variation did not overtly alter subcellular localization (Fig 2G). To identify DDX41-sensitive molecular processes in hi-*Ddx41*$^{+/-}$ cells that can be leveraged to quantitatively compare DDX41 and variant activities, RNA-seq was integrated into the rescue system (Fig. 2H). DDX41 expression in hi-*Ddx41*$^{+/-}$ cells significantly altered the abundance of a restricted ensemble of transcripts; 16 and 15 were upregulated and downregulated, respectively (Fig. 2H, left and Supplementary Table 1).

To prioritize candidates from among the DDX41-regulated transcripts, mouse-specific genes and predicted genes were excluded, and only genes with TPM >1 were considered. The transcripts were quantified in hi-*Ddx41*$^{+/-}$ cells, with or without DDX41 expression, to determine if DDX41 rescues transcript levels. Among these transcripts, we analyzed whether they were also regulated by DDX41 disease variants, and four were analyzed further (Fig. 2H, right). *Syndecan-1* (*Sdc1*) RNA was elevated 1.6-fold ($p = 0.0008$) in hi-*Ddx41*$^{+/-}$ versus hi-*Ddx41*$^{+/+}$ cells, and DDX41, but not the G173R and R525H variants, decreased its expression (68%, $p = 0.004$). *Fam133b, Clk3, and Gas5* mRNA levels were lower in hi-*Ddx41*$^{+/-}$ versus hi-*Ddx41*$^{+/+}$ cells. DDX41, but not the mutants, increased *Fam133b* mRNA levels (1.7-fold, $p = 0.0149$). DDX41 increased *Clk3* and *Gas5* mRNA levels 1.4- and 1.6-fold ($p = 0.0098$ and 0.0564), while the G173R variant was inactive; R525H had reduced activity (1.2–1.4-fold increase, $p = 0.1123$ and 0.2617).

To determine if the novel variants retain competence to alter the levels of DDX41-regulated transcripts, we conducted qRT-PCR with two primer sets that amplify distinct exons of each gene (Fig. 2I). *Sdc1* expression was 1.7-fold higher ($p < 0.0001$; E3–4, $p = 0.0194$; E4–5) in hi-*Ddx41*$^{+/-}$ versus hi-*Ddx41*$^{+/+}$ cells, and DDX41 decreased its expression. *Fam133b, Gas5,* and *Clk3* expression were 40–50% lower (*Fam133b*; $p = 0.0075$ (E6–7), $p < 0.0001$ (E7–8), *Gas5*; $p < 0.0001$ (E4–6 and E6–8), and *Clk3*; $p = 0.0009$ (E4–5), $p<0.0001$ (E9–10), respectively) in hi-*Ddx41*$^{+/-}$ versus hi-*Ddx41*$^{+/+}$ cells, and DDX41 rescued expression. Consistent with the RNA-seq data, G173R was inactive. R525H was not competent to regulate *Sdc1* and *Fam133b* mRNAs, and its activity to regulate *Clk3* and *Gas5* was attenuated (*Clk3*, 24% ($p = 0.1259$, E4–5) and 26% ($p<0.0001$, E9–10), *Gas5*, 30% ($p = 0.259$, E4–6) and 39% ($p < 0.0001$, E6–8) reduction). K331del variant did not alter the mRNA levels, and R293H variant activity was attenuated relative to DDX41 (*Sdc1*, 42% ($p < 0.0001$, E3–4) and 37% ($p = 0.0477$, E4–5), *Fam133b*, 44% ($p = 0.003$, E6–7) and 45% (p

= 0.0094, E7–8), *Clk3*, 29% (p = 0.0446, E4–5) and 40% (p < 0.0001, E9–10), *Gas5*, 45% (p = 0.022, E4–6) and 47% (p < 0.0001, E6–8) reduction).

We tested whether DDX41 and variants differed with respect to their activity to regulate hematopoietic differentiation in the genetic rescue assay. At an early stage of differentiation, although the wild type and heterozygous cells were morphologically indistinguishable (Supplementary Fig. 3), changes in cell surface markers were detectable by flow cytometry (Fig. 2J, Supplementary Fig. 4). The immortalized progenitor cells have the potential to undergo monocytic and granulocytic differentiation [12]. *Ddx41* haploinsufficiency increased monocytic differentiation ($CD11b^+CD115^+$; 2.2-fold increase, $p < 0.0001$). DDX41 expression in hi-$Ddx41^{+/-}$ cells reduced the monocytic population ($CD11b^+CD115^+$; 40% relative to control retrovirus-infected hi-$Ddx41^{+/-}$, $p < 0.0001$), while promoting granulocytic differentiation ($CD11b^+CD115^-$; 1.3-fold increase, $p < 0.0001$). However, the K331del and G173R variants lacked activity. DDX41, R525H, and G610S exhibited comparable activities ($CD11b^+CD115^+$; 30% (R525H, $p = 0.0012$) and 50% (G610S, $p < 0.0001$) reduction relative to control retrovirus-infected hi-$Ddx41^{+/-}$, $CD11b^+CD115^-$; 1.2-fold (R525H, $p = 0.001$) and 1.5-fold (G610S, $p < 0.0001$) increase). Thus, the germline K331del and G173R variants were overtly defective, whereas G610S, a variant of uncertain significance (Supplementary Fig. 5) retained activity, and the common somatic variant R525H retained a subset of activities. This genetic rescue-based differentiation assay complements the transcript quantification assay for curating functional attributes of human *DDX41* variants.

In conclusion, we developed a genetic rescue assay that quantitatively discriminated activities of DDX41 and myeloid malignancy-associated DDX41 genetic variants. Our analyses revealed that the variants were impaired in their intrinsic RNA-regulatory activities and to induce monocytic differentiation markers. It will be instructive to extend these analyses to more broadly conduct structure/function assessments for clinical genetic curation and leverage the quantitative assay to elucidate mechanisms and interventions that promote and/or oppose DDX41 function, thereby influencing DDX41-dependent pathogenicity.

Material and Methods

Patients and data collection

Families 1 and 2 were identified in University of Wisconsin/UW Health Hereditary Hematology and Bone Marrow Failure Clinic. Informed consent was obtained from probands and available close relatives or their healthcare proxy for deceased individuals. *DDX41* germline variants were identified through CLIA-certified clinical genetic testing and confirmed and segregated in available family members via Sanger sequencing. Medical and family history were obtained by patient and family member interviews and medical record review. This study was approved by University of Wisconsin-Madison Health Sciences Institutional Review Board and conducted in accordance with the Declaration of Helsinki.

Experimental model and methods

Protein structure prediction—AlphaFold was used to predict DDX41 structure. The DDX41 model was obtained from AlphaFold database (AF-Q9UJV9). DDX41 mutant structural models were generated with AlphaFold v2.1.0 Colab.

HoxB8-immortalized (hi)-*Ddx41* heterozygous mutant (*Ddx41*$^{+/-}$) cells—To generate HoxB8-immortalized (hi)-*Ddx41* mutant progenitors, CRISPR/Cas9 RNP complexes were introduced individually by electrophoresis into hi-WT progenitors described previously[12]. ER-HoxB8-immortalized (hi)- hematopoietic progenitors were generated by retroviral infection of estrogen-regulated HoxB8 into primary Lin$^-$ cells isolated from E14.5 mouse fetal liver. The sex of the cells was male, identified by PCR analysis of the *DDX3y* gene with genomic DNA. For targeting *Ddx41*, three crRNAs (A;5'-AGATGAGGACGACATCCCGC-3', B;5'- TGATCGGCATTGCCTTCACG-3', and C;3'-ATGCTCAGGACATAACGCGG-5', Integrated DNA Technologies; Coralville, IA, USA) targeting distinct exons were annealed to tracrRNA to generated guide RNAs which were then assembled into RNP complexes with sNLS-spCas9-sNLS (Aldevron (Madison, WI, USA). Each RNP complex was introduced into 2×10^5 hi-progenitor cells using 4D-Nucleofector™ with P3 Primary Cell 4D-Nucleofector® X Kit (Lonza; Basel, Switzerland). 72 hours post-electroporation, clones were isolated by limiting dilution (0.5 cell/well of a 96-well plate). Clones were cultured until colonies became visible and where then transferred to larger wells. Sanger sequencing of genomic DNA was used to establish genotypes, and sequencing data was analyzed by SnapGene Viewer (San Diego, CA, USA). Cells were cultured in OPTI-MEM supplemented with 10% FBS, 1% penicillin-streptomycin, 1% SCF-conditioned medium, 28.6 μM β-mercaptoethanol, 1 μM β-estradiol, and 400 μg/ml G418 in a humidified 5% CO_2 incubator at 37–C.

DDX41 rescue assay—DDX41 and human myeloid malignancy-associated DDX41 variants were expressed from the MSCV-PIG retroviral expression vector. Retroviruses were packaged in 293T cells and retrovirus-containing supernatants were collected 48h post-transfection. hi-*Ddx41*$^{+/+}$ and hi-*Ddx41*$^{+/-}$ hematopoietic progenitors were infected with retrovirus expressing GFP alone or GFP and DDX41 (WT or variants). Cells were transferred to IMDM containing 2% FBS and incubated with infectious supernatant by spinoculation for 90 min at 2,800 rpm at 30°C. Cells were cultured for 2 days in immortalized cell culture media described above. GFP$^+$ cells were isolated by fluorescence-activated cell sorting with FACSAria cell sorter (BD Biosciences; Franklin Lake, NJ, USA). RNA and protein of sorted GFP-positive cells was analyzed by RNA-seq, RT-qPCR and semi-quantitative Western blotting.

Semi-quantitative Western blotting—Cells were washed with ice-cold PBS and boiled for 10 min in 2x sodium dodecyl sulfate (SDS) lysis buffer (50 mM Tris (pH 6.8), 2% β-mercaptoethanol, 2% SDS, 0.1% bromophenol blue, 10% glycerol). Proteins were analyzed by western blotting with ECL 2 (Thermo Fisher Scientific; Waltham, MA, USA) and West Femto (Thermo Fisher Scientific) with rabbit monoclonal anti-Flag (Cell Signaling Technology; Danvers, MA, USA), mouse monoclonal anti-DDX41 (Novus Bioscience; Littleton, CO, USA), rabbit polyclonal anti-DDX41 antibody generated against purified full-

length DDX41 protein (Cocalico Biologicals, Inc.; Stevens, PA, USA), mouse monoclonal anti-β-actin (Cell Signaling Technology) or anti-GAPDH (Cell Signaling Technology). Blots were developed using LI-COR Odyssey Imaging System (LI-COR Biosciences; Lincoln, NE, USA) and quantified by Image Studio Lite (version 5.2.5) (LI-COR Biosciences). Quantification is represented as mean with SD. Statistical analyses were conducted using ANOVA tests (significance cutoff of p value <0.05) as calculated using Prism software (GraphPad Software; San Diego, CA, USA).

Immunofluorescence—hi-*Ddx41*$^{+/+}$ cells were infected with empty retrovirus or retroviruses expressing DDX41 or variants, collected on poly-L-lysine coated slides (Electron Microscopy Sciences; Hatfield, PA, USA) and fixed with 3.7% paraformaldehyde in PBS for 10 min at room temperature. Slides were washed with PBS and permeabilized with 0.2% Triton X-100 for 10 min at room temperature. Washed slides were blocked with 3% BSA in PBS containing 0.1% Tween 20 for 1 h at room temperature and incubated with rabbit anti-Flag (Cell Signaling Technology) in 3% BSA at 4–C overnight. After washing, slides were incubated with Alexa 594 secondary antibody (Invitrogen; Waltham, MA, USA) for 1 h at room temperature, washed and mounted using Vectashield mounting medium with DAPI (Vector Laboratories; Burlingame, CA, USA). Images were acquired with a Nikon A1R-S confocal microscope (Nikon; Minato City, Tokyo, Japan).

RNA-seq with DDX41 rescue assay—Three biological replicates of hi-*Ddx41*$^{+/+}$ cells infected with empty vector and hi-*Ddx41*$^{+/-}$ cells infected with empty vector or retroviruses expressing DDX41 or G173R or R525H were harvested and sorted for GFP^{+} cells on a FACSAria II instrument (BD Biosciences). RNA was purified using an RNAeasy Micro Kit (Qiagen; Hilden, Germany). Library sequencing through Illumina TruSeq Stranded Total RNA (rRNA reduction) was conducted by the University of Wisconsin-Madison Gene Expression Center and sequenced using an Illumina NovaSeq 6000. Reads were aligned by STAR (version 2.5.2b) to the mouse genome (version mm39) with GENCODE basic gene annotations (version M22). Gene expression levels were quantified by RSEM (version 1.3.0), and differential expression was analyzed by edgeR (version 3.30.3).

qRT-PCR—Total RNA was purified from 2–5 × 10^5 cells with TRIzol (Invitrogen) and 1–2 μg RNA was treated with DNase I (Thermo Fisher Scientific) for 15 min at room temperature. After heat inactivation of DNase I with EDTA for 10 min at 65°C, 0.5–1μg RNA was incubated with a 4:1 mixture of oligo(dT) primers and random hexamer at 68°C for 10 min. RNA/primers were incubated with Moloney murine leukemia virus reverse transcription (M-MLV RT) (Thermo Fisher Scientific), 5X first strand buffer (Thermo Fisher Scientific), 10 mM dithiothreitol (Thermo Fisher Scientific), RNAsin (Promega), and 0.5 mM deoxynucleoside triphosphates (New England Biolabs; Ipswich, MA, USA) at 42°C for 1 h and then heat inactivated at 95°C for 5 min. Quantitative gene expression analyses were conducted by real-time RT-PCR using Power SYBR Green Master Mix (Applied Biosystems; Waltham, MA, USA) and analyzed on a ViiA 7 Real-Time PCR System (Applied Biosystems). Control reactions without M-MLV RT yielded little to no signal. Relative expression of mRNA was determined from a standard curve of serial dilutions of cDNA samples, and values were normalized to *Hprt* RNA expression. Quantitative RT-PCR

results were presented as box and whisker plots. Statistical comparisons were conducted using ANOVA test (significance cutoff of P value <0.05) as calculated using Prism software (GraphPad Software).

Cell differentiation and flow cytometry—hi-*Ddx41*$^{+/+}$ and hi-*Ddx41*$^{+/-}$ cells were infected with retroviruses expressing DDX41 or variants. One day post-infection, cells were washed with ice-cold PBS and resuspended in differentiation medium (OPTI-MEM supplemented with 10% FBS, 1% penicillin-streptomycin, 1% SCF-conditioned medium, 1% IL-3-conditioned medium, and 28.6 μM β-mercaptoethanol). Cells were cultured for 3 days at 37–C. For analysis of monocytic and granulocytic populations by flow cytometry, cells were washed with ice-cold PBS containing 2% FBS and 2mM EDTA, and live/dead cell staining was conducted using Ghost Red Dye 780 (Tonbo Biosciences, San Diego, CA, USA) at 4–C for 15 min, followed by washing with PBS containing 2% FBS and 2 mM EDTA. Surface antigens were stained using 1:200 diluted combinations of APC-CD11b (BioLegend) and PE-CD115 (BioLegend) in PBS with 2% FBS and 2 mM EDTA at 4–C for 30 min. After staining, cells were washed with ice-cold PBS containing 2% FBS and EDTA, and analyzed on an Attune™ NxT Flow Cytometer (Thermo Fisher Scientific). Differentiated cell populations were analyzed using FlowJo v10.8.0 software (BD Biosciences).

Supplementary Material

Refer to Web version on PubMed Central for supplementary material.

Acknowledgements

This work was supported by Edward Evans Foundation grant, NIH DK68634 and NIH P30CA014520.

References

1. Tawana K, Brown AL, Churpek JE. Integrating germline variant assessment into routine clinical practice for myelodysplastic syndrome and acute myeloid leukaemia: current strategies and challenges. Br J Haematol 2021 Oct 18.
2. Irion U, Leptin M. Developmental and cell biological functions of the Drosophila DEAD-box protein abstrakt. Curr Biol 1999 Dec 2; 9(23): 1373–1381. [PubMed: 10607561]
3. Polprasert C, Schulze I, Sekeres MA, Makishima H, Przychodzen B, Hosono N, et al. Inherited and Somatic Defects in DDX41 in Myeloid Neoplasms. Cancer Cell 2015 May 11; 27(5): 658–670. [PubMed: 25920683]
4. Zhang Z, Yuan B, Bao M, Lu N, Kim T, Liu YJ. The helicase DDX41 senses intracellular DNA mediated by the adaptor STING in dendritic cells. Nat Immunol 2011 Sep 4; 12(10): 959–965. [PubMed: 21892174]
5. Weinreb JT, Ghazale N, Pradhan K, Gupta V, Potts KS, Tricomi B, et al. Excessive R-loops trigger an inflammatory cascade leading to increased HSPC production. Dev Cell 2021 Mar 8; 56(5): 627–640 e625. [PubMed: 33651979]
6. Chlon TM, Stepanchick E, Hershberger CE, Daniels NJ, Hueneman KM, Kuenzi Davis A, et al. Germline DDX41 mutations cause ineffective hematopoiesis and myelodysplasia. Cell Stem Cell 2021 Nov 4; 28(11): 1966–1981 e1966. [PubMed: 34473945]
7. Jumper J, Evans R, Pritzel A, Green T, Figurnov M, Ronneberger O, et al. Highly accurate protein structure prediction with AlphaFold. Nature 2021 Aug; 596(7873): 583–589. [PubMed: 34265844]

8. Sebert M, Passet M, Raimbault A, Rahme R, Raffoux E, Sicre de Fontbrune F, et al. Germline DDX41 mutations define a significant entity within adult MDS/AML patients. Blood 2019 Oct 24; 134(17): 1441–1444. [PubMed: 31484648]

9. Lewinsohn M, Brown AL, Weinel LM, Phung C, Rafidi G, Lee MK, et al. Novel germ line DDX41 mutations define families with a lower age of MDS/AML onset and lymphoid malignancies. Blood 2016 Feb 25; 127(8): 1017–1023. [PubMed: 26712909]

10. Kadono M, Kanai A, Nagamachi A, Shinriki S, Kawata J, Iwato K, et al. Biological implications of somatic DDX41 p.R525H mutation in acute myeloid leukemia. Exp Hematol 2016 Aug; 44(8): 745–754 e744. [PubMed: 27174803]

11. Churpek JE, Smith-Simmer K. DDX41-Associated Familial Myelodysplastic Syndrome and Acute Myeloid Leukemia. In: Adam MP, Mirzaa GM, Pagon RA, Wallace SE, Bean LJH, Gripp KW, et al. (eds). GeneReviews((R)): Seattle (WA), 2021.

12. Johnson KD, Conn DJ, Shishkova E, Katsumura KR, Liu P, Shen S, et al. Constructing and deconstructing GATA2-regulated cell fate programs to establish developmental trajectories. J Exp Med 2020 Nov 2; 217(11)

13. Katsumura KR, Mehta C, Hewitt KJ, Soukup AA, Fraga de Andrade I, Ranheim EA, et al. Human leukemia mutations corrupt but do not abrogate GATA-2 function. Proc Natl Acad Sci U S A 2018 Oct 23; 115(43): E10109–E10118. [PubMed: 30301799]

14. Cavalcante de Andrade Silva M, Katsumura KR, Mehta C, Velloso E, Bresnick EH, Godley LA. Breaking the spatial constraint between neighboring zinc fingers: a new germline mutation in GATA2 deficiency syndrome. Leukemia 2021 Jan; 35(1): 264–268. [PubMed: 32286542]

15. Singh RS, Vidhyasagar V, Yang S, Arna AB, Yadav M, Aggarwal A, et al. DDX41 is required for cGAS-STING activation against DNA virus infection. Cell Rep 2022 May 24; 39(8): 110856. [PubMed: 35613581]

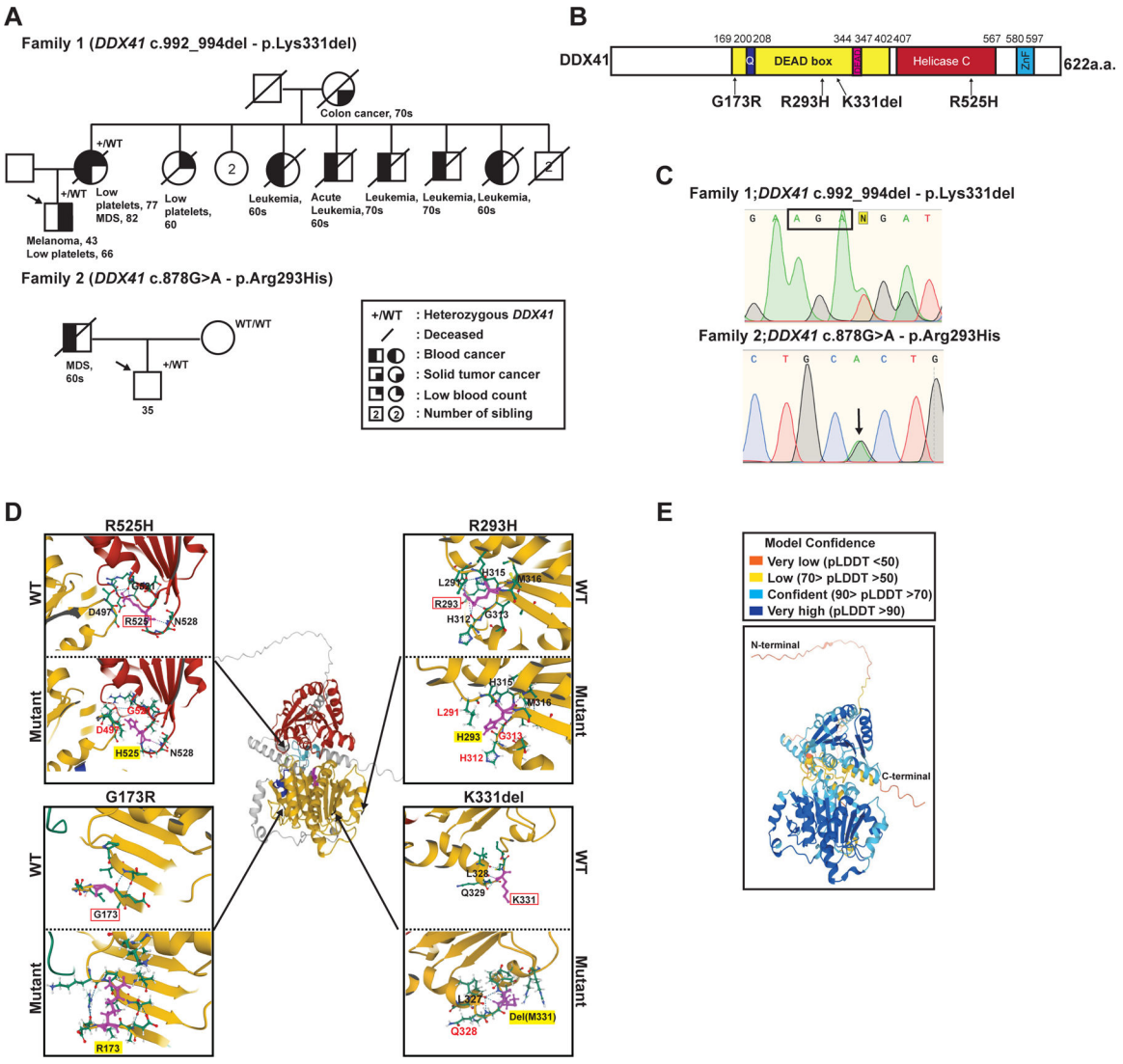

Fig. 1: Family histories and structural predictions of myeloid malignancy-associated *DDX41* variants.

A K331del and R293H pedigrees. Probands are indicated with an arrow. **B** Domain structure of human DDX41. Germline and somatic mutations are indicated within the corresponding domains. **C** Sanger sequencing data of probands in each family. **D** Predicted structure of mutant human DDX41 by AlphaFold[7] and 3-D images are created using Mol* viewer (https://molstar.org/viewer/). The residues forming the hydrogen bond and surrounding residues are indicated in black. Residues where this interaction is lost due to mutation are indicated in red. **E** Confidence of predicted structure from AlphaFold analysis.

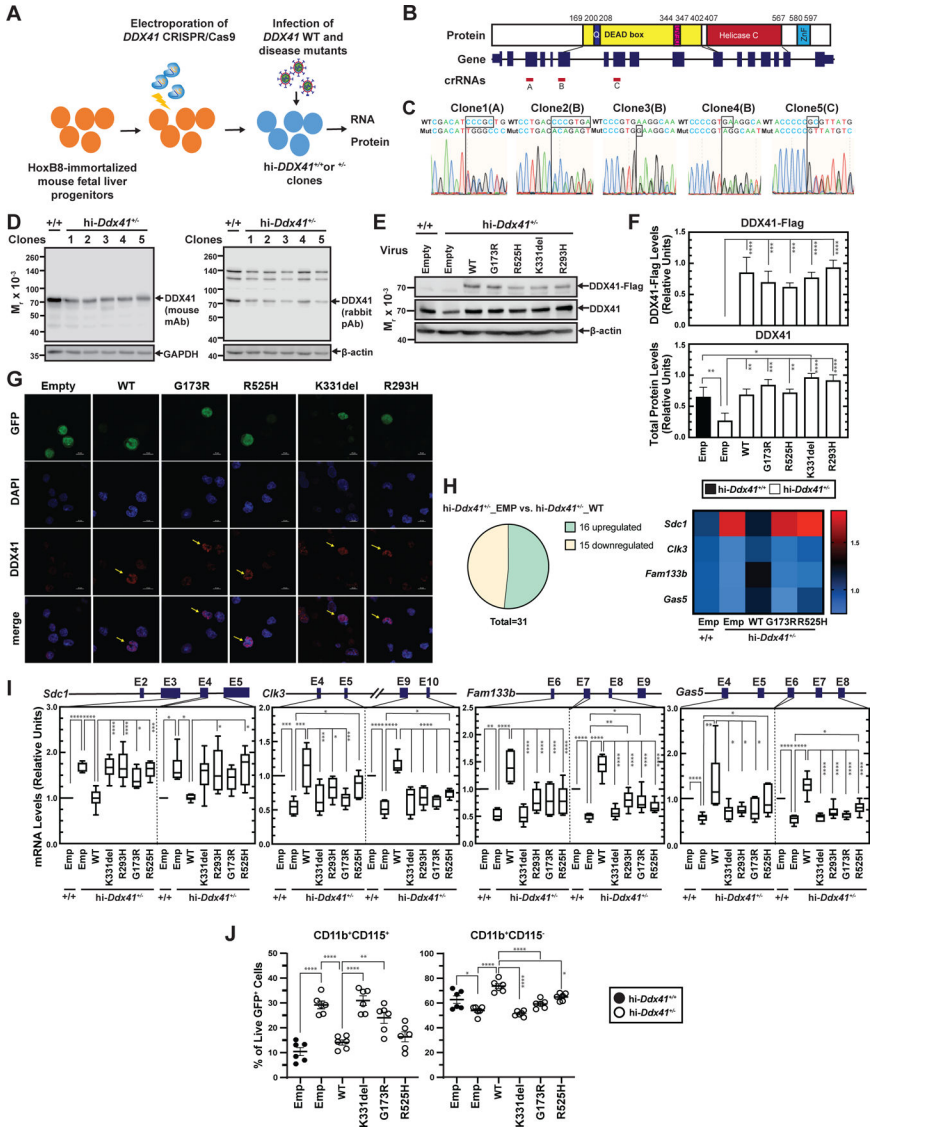

Fig. 2: Quantitative genetic rescue assay discriminates DDX41 and human myeloid malignancy-associated variant activities.

A Genetic rescue system. Three CRISPR/Cas9 RNP complexes for *Ddx41* were electroporated individually into HoxB-immortalized (hi)-progenitors, and clonal lines were isolated. Retrovirus expressing GFP or GFP and *DDX41* or a human disease-associated *DDX41* variant were infected into hi-*Ddx41*$^{+/+}$ and hi-*Ddx41*$^{+/-}$ cells. GFP-positive cells were isolated by flow cytometry and analyzed by qRT-PCR and RNA-seq. Protein was analyzed by semi-quantitative western blotting. **B** Exons corresponding to representative domains and target loci of crRNAs on murine *Ddx41*. **C** Sanger sequencing of genomic DNA at the edited region of hi-*Ddx41*$^{+/-}$ clonal lines. The crRNA used to generate each clone is indicated in parenthesis. **D** DDX41 protein levels in hi-*Ddx41*$^{+/+}$ and hi-*Ddx41*$^{+/-}$ cells were analyzed by semi-quantitative Western blotting using two different antibodies (mouse monoclonal anti-DDX41 antibody (2F4), Novus Biologicals, and our rabbit polyclonal anti-DDX41 antibody). Each clone number indicated corresponds to each

clone in Fig. 2C. **E** Representative Western blots of Flag-tagged DDX41 and variants and endogenous DDX41 using anti-DDX41 antibody in genetic rescue assay. **F** Quantitative analysis of DDX41 protein of Fig. 2E (n=3 per group). **G** Subcellular localization of DDX41 and variants by confocal fluorescence microscope using anti-Flag antibody. **H** mRNAs regulated by DDX41 genetic rescue in hi-*Ddx41*$^{+/-}$ cells. Heatmap with TPM values of DDX41-regulated mRNAs from total RNA-Seq (n=3 per group). **I** qRT-PCR analysis of DDX41-regulated mRNAs (n=6 per group). Statistics were calculated using one-way ANOVA, followed by Tukey's test; *, $P \leq 0.05$; **, $P \leq 0.01$; ***, $P \leq 0.001$; ****, $P \leq 0.0001$. **J** Monocytic and granulocytic populations of live GFP^{+} cells with CD11b and CD115 surface markers detected by flow cytometry (n=6 per group). Statistics were calculated using one-way ANOVA, followed by Tukey's test; *, $P \leq 0.05$; **, $P \leq 0.01$; ***, $P \leq 0.001$; ****, $P \leq 0.0001$.

Primer sequences

Target gene	sequence
DDX41 Exon9-Forward	ATCATCTGCCCCTCGGTAAG
DDX41 Exon9-Reverse	CCCCAACTAACCTCCCCATT
DDX41 Exon10-Forward	ATACATAGGGCAGGTGGTGG
DDX41 Exon10-Reverse	AGCTGAGCAACTGAGACACA
Sdc1-exon3_4-Forward	GAGGATGGAACTGCCAATCA
Sdc1-exon3_4-Reverse	CCCAGATGTTTCAAAGGTGAAG
Sdc1-exon4_5-Forward	GGTGCTTCTCAGAGCCTTT
Sdc1-exon4_5-Reverse	AGGCACACAGCAAAGATGA
Clk3-exon4_5-Forward	GGCGATTGGCTCCAAGA
Clk3-exon4_5-Reverse	AGCACTCCACCACCTTG
Clk3-exon9_10-Forward	CCATGAACATCACACCACCA
Clk3-exon9_10-Reverse	CTCAAAGAGAATGCAGCCGATA
Fam133b-exon6_7-Forward	TCTGATTCTTCCAGCAGTTCTT
Fam133b-exon6_7-Reverse	AGGAGACTTATGGCAACGG
Fam133b-exon7_8-Forward	CGTTGCCATAAGTCTCCTGA
Fam133b-exon7_8-Reverse	TTTCTCTTTCAGTTACATCCTTGG
Gas5-exon4_6-Forward	GTCAGGAAGCTGGATAACAGAG
Gas5-exon4_6-Reverse	AGCCTCAAACTCCACCATTT
Gas5-exon6_8-Forward	GGTGGAGTTTGAGGCTGGATA
Gas5-exon6_8-Reverse	CCAAGCAAGCCAGCCAA

Key Resource Table

Reagent	Source	Identifier
Bacterial strains		
JM109 competent cells	Promega	L2001
Experimental model: Cell lines		
Mouse: hi-*Ddx41*$^{+/+}$ and hi-*Ddx41*$^{+/-}$cells	This paper	N/A
CRISPR/Cas-9 system		
Predesigned Alt-R CRISPR-Cas9 gRNA for mouse *Ddx41*	Integrated DNA Technologies	Mm.Cas9.DDX41.1.AA, Mm.Cas9.DDX41.1.AB, Mm.Cas9.DDX41.1.AC
sNLS-spCas9-sNLS	Aldevron	9212
Antibodies		
Flag-tag rabbit mAb	Cell Signaling Technology	14793
Alexa Fluor 594 chicken anti-rabbit IgG (H+L)	Invitrogen	A21442
DDX41 mouse mAb	Novus Biologicals	H00051428-M01
DDX41 rabbit pAb	Cocalico Biologicals, INC.	Bresnick laboratory-generated
β-actin mouse mAb	Cell Signaling Technology	3700S
GAPDH rabbit mAb	Cell Signaling Technology	2118
Recombinant DNA		
pMSCV-PIG	Mitchell Weiss (St. Jude Children's Research Hospital)	N/A
pMSCV-PIG-DDX41 WT	This paper	N/A
pMSCV-PIG-DDX41-G173R pMSCV-PIG-DDX41-R293H pMSCV-PIG-DDX41-K331del pMSCV-PIG-DDX41-R525H	This paper	N/A
Chemicals		
Pierce™ ECL 2 Western Blotting Substrate	Thermo Fisher Scientific	80196
SuperSignal™ West Femto Maximum Sensitivity Substrate	Thermo Fisher Scientific	34096
Power SYBR Green Master Mix	Applied Biosystems	4367659
TRIzol Reagent	Thermo Fisher Scientific	15596
Phusion High-Fidelity DNA Polymerase	Thermo Fisher Scientific	F530S
P3 Primary Cell 4D-Nucleofector® X Kit	Lonza	V4XP-3032
Critical commercial kit		
RNAeasy Micro Kit	Qiagen	74004
QIAquick Gel Extraction Kit	Qiagen	28706
QIAquick PCR Purification Kit	Qiagen	28106
Software		
Image Studio Lite (version 5.2)	Image studio acquisition software	https://www.licor.com/
Prism 9	GraphPad	https://www.graphpad.com/
SnapGene viewer	Dotmatics	https://www.snapgene.com/snapgene-viewer/